



Chloride-induced corrosion of steel rebars in simulated pore solutions of alkali-activated concretes



Shishir Mundra^a, Maria Criado^a, Susan A. Bernal^b, John L. Provis^{a,*}

^a Department of Materials Science and Engineering, The University of Sheffield, Sir Robert Hadfield Building, Sheffield S1 3JD, United Kingdom

^b Department of Civil and Structural Engineering, The University of Sheffield, Sir Frederick Mappin Building, Sheffield S1 3JD, United Kingdom

ARTICLE INFO

Keywords:

Chloride (D)

Corrosion (C)

Electrochemical properties (C)

Pore solution (B)

Alkali activated cement (D)

ABSTRACT

The passivation and chloride-induced depassivation of steel rebars immersed in varying alkaline environments (0.80 M, 1.12 M and 1.36 M NaOH solutions), simulating the pore solutions of low-Ca alkali-activated concretes, were investigated using a range of electrochemical techniques. The passive film on the steel rebars was complex in chemical makeup, composed of Fe-hydroxides, oxy-hydroxides and oxides. An increased degree of passivation of the rebars was observed when exposed to solutions with higher hydroxide concentrations. The critical chloride level ($[\text{Cl}^-]/[\text{OH}^-]$ ratio) required to induce depassivation of steel was strongly dependent on the alkalinity of the pore solution, and was found to be 0.90, 1.70 and 2.40 for 0.80 M, 1.12 M and 1.36 M NaOH solutions, respectively. These values all correspond to a constant value of $[\text{Cl}^-]/[\text{OH}^-]^3 = 1.25$, which is a novel relationship to predict the onset of pitting, interlinking chloride concentration and the solubility of the passive film.

1. Introduction

In hydrated cement pastes, where the pore solution is characterised by high alkalinity (pH between 12.5 and 14), a thermodynamically stable passive film [1,2] is formed on the steel rebars, protecting the underlying metal from the action of aggressive species such as chloride, and slow the growth of corrosion products [3]. The passive film formed on the surface of the reinforcement comprises iron oxides such as $\alpha\text{-Fe}_2\text{O}_3$, $\gamma\text{-Fe}_2\text{O}_3$, Fe_3O_4 , and iron hydroxides and oxy-hydroxides such as $\text{Fe}(\text{OH})_2$, $\text{Fe}(\text{OH})_3$, $\alpha\text{-FeOOH}$, $\gamma\text{-FeOOH}$ and $\beta\text{-FeOOH}$, with a layered microstructure [4–9]. The chemistry of the passive film is governed by the oxygen availability, pH and chemistry of the surrounding environment, and the redox potential of the steel [4–8]. In concrete environment, breakdown of the passive film or ‘depassivation’ can be initiated by two common mechanisms: the lowering of pH, e.g. due to carbonation, and by the localised attack of aggressive species such as chloride.

The breakdown of passivation due to the action of chloride is often associated with the concept of critical chloride value or chloride ‘threshold’ value (C_{crit}); defined as the minimum amount of chloride at the steel-concrete interface which is required to initiate depassivation of the reinforcement [10]. The C_{crit} value is influenced by a large number of factors, including: the chemistry and alkalinity of the pore solution [8,11–17], chloride binding in the cement hydrates [18–20],

the steel-concrete interface [21], the availability of oxygen at the steel-concrete interface [22] and the surface condition and chemical composition of the reinforcement [11,14]. Given the number of confounding variables, there exists no general consensus on a precise chloride ‘threshold’ value [10]. In an extensive review, Angst et al. [10] summarised the C_{crit} values obtained by several authors to be between 0.04 wt% and 8.34 wt% of the binder, and between 0.01 and 45 in terms of the molar ratio $[\text{Cl}^-]/[\text{OH}^-]$. These values correspond to systems based primarily on Portland cement (PC), and were determined through electrochemical measurements conducted on in-service structures, simulated pore solutions and laboratory specimens.

Alkali-activated materials (AAMs) are a class of cementitious binders that have gained significant academic and industrial interest over the past decades as an alternative to PC for production of concretes. These materials have the potential to achieve significant reductions in greenhouse emissions and present performance advantages, in some applications, compared to PC [23–25]. AAMs are defined as the product of the reaction between solid aluminosilicate powders (generally industrial by-products such as fly ash or blast furnace slag; or calcined clays) and alkaline activators (often an aqueous solution of alkali metal silicate or hydroxide) [25,26]. AAMs can be characterised, according to the calcium content in the binding material, into two broad categories: high-calcium systems such as alkali-activated slags where the reaction product is dominated by a calcium-aluminosilicate hydrate (C-A-S-H)

* Corresponding author.

E-mail address: j.provis@sheffield.ac.uk (J.L. Provis).

<http://dx.doi.org/10.1016/j.cemconres.2017.08.006>

Received 2 October 2016; Received in revised form 6 August 2017; Accepted 8 August 2017

Available online 12 August 2017

0008-8846/ © 2017 The Authors. Published by Elsevier Ltd. This is an open access article under the CC BY-NC-ND license (<http://creativecommons.org/licenses/by-nc-nd/4.0/>).

gel; and low-Ca systems such as alkali-activated fly-ash/metakaolin where the main reaction product is a poorly crystalline three dimensional alkali-aluminosilicate hydrate (N-A-S-H) gel. The composition of the pore solution at the steel-concrete interface in AAMs is significantly different from that of PC-based concretes, due to differences between the composition and mineralogy of these binders.

This study focuses on low-Ca AAMs, and specifically the simulation of pore solutions present within these binders. In the pore solutions associated with neat PC hydrates [27], alkali and hydroxide concentrations are about 0.70 M, while concentrations of calcium and sulfate are around 2 mM and 7 mM respectively, with Si and Al each present at levels of less than 1 mM [27]. However, this composition would vary with time and composition of the precursors. The pore solutions of low-Ca AAMs are more alkaline than those of PC pore solutions. Lloyd et al. [28] measured the concentrations of different species in pore solutions extracted from alkali-activated fly ashes and observed concentrations of Na^+ and OH^- between 0.60 M and 1.60 M, respectively. Sulfate was not detected, and the concentrations of Ca, Si and Al were close to 1 mM [28,29]. These differences in the hydration products and pore solution of low-Ca AAMs in contact with the reinforcement, compared to PC based concretes, could lead to dissimilar mechanisms of passivation (and passivation breakdown) due to the ingress of chloride.

There are limited published data on the chloride induced corrosion of reinforcement in low-Ca AAMs. Miranda et al. [30] and Bastidas et al. [31] reported similar passivation behaviours for alkali-activated fly ash and PC mortars, however upon addition of chloride (2 wt% of binder), increased corrosion current density and lower corrosion resistance were observed for alkali activated fly ash mortars than PC mortars. Criado et al. [32] indicated that depassivation of carbon steel rebar in alkali-activated fly ash mortars could be initiated at a chloride content of around 0.4 wt% of binder, but this value depended on the activator used. However, Monticelli et al. [33] reported C_{crit} values for alkali-activated fly ash mortars to be about 1–1.7 wt% of binder, much higher than previously reported. With such limited and varying data in the literature related to degradation of the reinforcement in AAMs, and considering the significant differences from reinforced PC concretes (as shown by Babaee and Castel [34]), it is important to gain an understanding of the mechanisms responsible for passivation of the reinforcement and its breakdown due to chloride.

This study investigated the passivation behaviour of steel and the phenomena of localised corrosion due to chlorides in highly alkaline electrolyte solutions (0.80 M, 1.12 M and 1.36 M NaOH) representing the pore solutions of low-Ca AAMs, with the aim of probing the chloride ‘threshold’ values for such systems. This was achieved by employing electrochemical techniques such as cyclic voltammetry (CV), open circuit potential (OCP), alternating current electrochemical impedance spectroscopy (EIS), linear polarisation resistance (LPR) and anodic polarisation.

2. Experimental programme

2.1. Materials

Mild steel rebars ($\varphi = 12$ mm) were obtained from a local supplier in Sheffield, UK. The rebars were sectioned into small pellets, thickness 5.5–6.5 mm, using an abrasive disc. Before electrochemical testing, the pellet surfaces were polished using SiC abrasive paper with 240 to 600 grit sizes and degreased using acetone. The chemical composition of the rebar, measured by X-ray fluorescence (XRF), is shown in Table 1.

The compositions of the simulated pore solutions were based on the work of Lloyd et al. [28] who analysed the pore solution chemistry of alkali-activated fly ashes. The concentrations of dissolved Al, Si, Ca and sulfur species in that study were close to or less than 1 mM, therefore were not considered here. In addition, preliminary tests with pore solutions containing Al, Si and Ca in concentrations of 3 mM, 0.9 mM and

Table 1
Composition of mild steel rebar measured using XRF (standard deviation = ± 0.03).

Elements	Fe	C	Cr	Ni	Cu	Si	Mn	S	Mo	P
wt%	97.91	0.21	0.13	0.20	0.47	0.23	0.76	0.03	0.02	0.04

0.45 mM respectively [35], showed negligible or no differences in the electrochemical response of the system. Alkali hydroxide solutions were used to simulate the pore solution chemistry of these binders: sodium hydroxide solutions with $[\text{OH}^-]$ concentrations of 0.80 M, 1.12 M and 1.36 M were prepared using ACS reagent grade NaOH pellets (Sigma Aldrich). To investigate the effect of chloride on corrosion initiation, commercial grade NaCl (EMD Chemicals) was added to the representative pore solutions; the molar ratio $[\text{Cl}^-]/[\text{OH}^-]$ was varied between 0 and 3 for each of the three NaOH concentrations assessed. Table 2 lists the aqueous compositions considered in this study.

2.2. Electrochemical techniques

All electrochemical tests were conducted in a 400 mL corrosion cell using a PGSTAT 204 potentiostat/galvanostat (Metrohm Autolab B.V.). Measurements were conducted using a conventional three electrode setup (electrolyte volume 250 mL), comprising a stainless steel counter electrode, an Ag/AgCl (filled with 3 M KCl) reference electrode and the steel surface (surface area: 0.287 cm²) acting as the working electrode. The reference electrode was positioned near the surface of the working electrode by means of a Luggin capillary. All measurements were conducted at room temperature (22 ± 2 °C) at least on two samples to ensure reproducibility.

2.2.1. Cyclic voltammetry

Potentiostatic cyclic voltammetry (CV) was conducted to electrochemically characterise the passive film formed on the steel surface when exposed to the three NaOH concentrations without chlorides (0.80 M, 1.12 M and 1.36 M NaOH solutions). Before starting each test, the steel was maintained at -1.50 V vs. Ag/AgCl (cathodic limit: $E_{\lambda,c}$) in the hydrogen evolution region for 10 min to remove the pre-existing oxide layers on the surface of steel. The electrochemical response of the system was recorded when the potential was cycled from -1.50 V ($E_{\lambda,c}$) to 0.65 V (anodic limit: $E_{\lambda,a}$), at a scan rate of 2.5 mV/s over 10 cycles, taking into account hydrogen and oxygen evolution at the cathodic and anodic limits respectively.

2.2.2. Open circuit potential, electrochemical impedance spectroscopy, linear polarisation resistance and anodic polarisation

To investigate the role of chloride on corrosion initiation, the following electrochemical techniques were employed (in the order described) on the same steel specimen, which was distinct from the specimen used for CV, in each of the solutions listed in Table 2: (i) OCP or E_{corr} ; (ii) EIS; (iii) LPR; and (iv) anodic polarisation.

Prior to testing, each sample was allowed to stabilise in the electrolyte for 15 min inside the corrosion cell. The OCP was recorded for 30 min in the beginning of the experiment, unless the change in potential with time (dV/dt) reached ≤ 1 $\mu\text{V/s}$ before 30 min. The OCP value reported in each case is the mean potential recorded during the last 20 s of the test.

EIS measurements were conducted for selected specimens in galvanostatic mode, where the net current in the system was maintained at 0.00 A. The galvanostatic mode was chosen primarily to address any variation in the OCP due to the interaction of chloride with steel during the course of EIS measurements. The tests were carried out in the frequency range of 10^5 Hz– 10^{-2} Hz, with a logarithmic sweeping frequency of 50 points per decade and a current amplitude of 10^{-5} A (RMS), to ensure that the corresponding potential variation did not exceed 10 mV. The results were analysed only for impedance

Table 2Simulated low-Ca AAM pore solutions with varying alkalinity and chloride concentrations ($[\text{Cl}^-]/[\text{OH}^-]$ ratio). All concentrations in mol/L.

Molar ratio $[\text{Cl}^-]/[\text{OH}^-]$	0	0.25	0.50	0.75	0.80	0.90	1.00	1.50	1.60	1.70	2.00	2.30	2.40	3.00
[NaOH]	Concentration of chloride, mol/L													
0.80	0	0.20	0.40	0.60	0.64	0.72	0.80	1.20	–	–	1.60	–	–	2.40
1.12	0	0.28	0.56	0.84	–	–	1.12	1.68	1.79	1.90	2.24	–	–	3.36
1.36	0	0.34	0.68	1.02	–	–	1.36	2.04	–	–	2.72	3.13	3.26	4.08

measurements in the frequency range of $10^4 \text{ Hz} - 10^{-2} \text{ Hz}$, to eliminate the effects of the reference electrode and the Luggin capillary, observed at frequencies between 10^5 Hz and 10^4 Hz .

Prior to LPR measurements, the open circuit potential was measured once again to take into account any change in potential during EIS testing due to changes on the steel surface. The potential was varied from -20 mV to $+20 \text{ mV}$ vs. the new OCP (scan rate of 0.167 mV/s and step potential 0.244 mV) and the current response was recorded. The polarisation resistance (R_p) was calculated using the modified Stern-Geary equations, Eqs. (1) and (2):

$$R_p = \left(\frac{\Delta E}{\Delta I} \right)_{\Delta E \rightarrow 0} \quad (1)$$

$$i_{\text{corr}} = \frac{B}{R_p} \quad (2)$$

where ΔE and ΔI are the changes in potential and current respectively, i_{corr} is the corrosion current density (A/cm^2), and B is the proportionality constant (V). From Eq. (1), the polarisation resistance was calculated by measuring the slope of the E-I plot. Corrosion current densities were calculated using Eq. (2) from the measured R_p values, using proportionality constants B proposed in the literature [34,36].

The specimens were polarised in the anodic direction from new OCP to determine the chloride threshold value. The potential was varied from the new OCP to $+1.0 \text{ V}$ with the step potential and scan rate set at 0.244 mV and 0.167 mV/s respectively, and the corresponding current density was recorded.

3. Results and discussion

3.1. Passivation

3.1.1. Cyclic voltammetry

Fig. 1 shows 10 cyclic voltammetric scans obtained for polished mild steel surfaces exposed to simulated pore solutions representative of low-Ca AAMs, as a function of the hydroxide concentration in the solution. The initial increase in the potential from $E_{\lambda,c}$ to -1.20 V was characterised by a sharp increase in the current, and the evolution of hydrogen bubbles from the steel surface (not shown in Fig. 1). Moving from the active to the noble direction, four anodic current peaks were observed, at approximately -0.94 V (denoted Peak I), -0.89 V (Peak II), -0.72 V (Peak III) and -0.67 V (Peak III'). Sweeping in the reverse direction, three cathodic current peaks at about -0.96 V (Peak IV'), -1.05 V (Peak IV) and -1.14 V (Peak V) were noticeable. Less clearly defined peaks III' and IV' were present as broad shoulders on the positive potential sides of the asymmetric peaks III and IV, respectively. The potential sweep after peak III' (not shown in Fig. 1) in the anodic direction up to $E_{\lambda,a}$ was characterised by a constant anodic current of a relatively low value until 0.55 V , where the current was observed to rise sharply due to the oxygen evolution reaction. A similar trend was observed in the cathodic direction (not shown in Fig. 1) in approximately the same potential range after which a rise in the cathodic current was witnessed, leading to peaks IV' and IV. Cathodic and anodic peak potentials were approximately the same for all three concentrations of hydroxide assessed, and therefore the following discussion applied is general to Fig. 1A, B and C.

Peaks I and II occurred as a single broad peak centred at about

-0.94 V in the first scan, however, a clear distinction between peak I (centred at -0.94 V) and peak II (centred at -0.89 V) was observed upon subsequent anodic potential sweeps. The current density of peak I increased from scan 1 to scan 10, and this was more pronounced with increasing hydroxide concentrations. Current densities for peak II remained fairly constant for all concentrations of hydroxide; however, the overlapping nature of peaks I and II became more distinct at higher alkalinity.

The cyclic voltammograms shown in Fig. 1 clearly indicate that passivation of the steel surface is a complex mechanism involving several oxidation processes, representing a chemical gradient in the composition of the passive film. Each current peak represents an individual oxidation/reduction process occurring on the surface of the steel. It can be assumed that the cathodic treatment of the steel for 10 min in the hydrogen evolution region at $E_{\lambda,c}$ results in the removal of the pre-existing oxide scale from the specimen surface, so iron exists in the bare Fe^0 state prior to sweeping in the forward direction. A minor peak at -1.10 V is primarily attributed to the electrochemical displacement of hydrogen adsorbed on the electrode surface. The occurrence of anodic peaks I and II likely corresponds to the electro-oxidation of iron from Fe^0 to Fe^{2+} [37,38]. The direct dependency of current densities of peaks I and II on the alkalinity of the electrolyte, indicates the possible role of $[\text{OH}^-]$ in the appearance of these peaks. Therefore, it is likely that peaks I and II are associated with the formation of $\text{Fe}(\text{OH})_2$. Such behaviour is expected in alkaline solutions, and several passivation mechanisms have been proposed since the early 20th century [39]. One possible reaction route for peaks I and II in the electrolytes used in this study, describing the initial formation of Fe^{2+} , could be represented by the reactions described in the Eqs. (3) to (6), where the square brackets depict the intermediate species, and curly braces indicate species that may undergo changes with time.



Peak I could therefore be attributed to the adsorption of $[\text{Fe}(\text{OH})]_{\text{ads}}^+$ on the surface of the specimen through a two-step electron transfer process indicated in reactions (3) and (4). Kabanov et al. [38] and Schrebler Guzmán et al. [40,41] reported the first stage of passivation to be the formation of an electrochemically active adsorbed layer of $[\text{Fe}(\text{OH})]_{\text{ads}}$ through reaction (3). A similar mechanism for the formation of $[\text{Fe}(\text{OH})]_{\text{ads}}$ was suggested by Dražić and Hao [42].

The second step is characterised by the formation of $[\text{Fe}(\text{OH})]_{\text{ads}}^+$ through an electron transfer process, occurring predominantly due to the labile nature of $[\text{Fe}(\text{OH})]_{\text{ads}}$ [38,40–43]. The amount of adsorbed species, therefore, depends on the concentration of OH^- , and is reflected by the increasing anodic current densities corresponding to peak I with increasing NaOH concentration. Peak II can be assigned to the formation of $\text{Fe}(\text{OH})_2$ by the mechanisms indicated in reactions (5) and (6). Thus, the fact that peak II is more distinct from peak I in 1.12 M (Fig. 1B) and 1.36 M (Fig. 1C) NaOH solutions than 0.80 M (Fig. 1A) NaOH solution could be explained by either the higher amounts of adsorbed $[\text{Fe}(\text{OH})]_{\text{ads}}^+$ or by the increased tendency to form HFeO_2^-

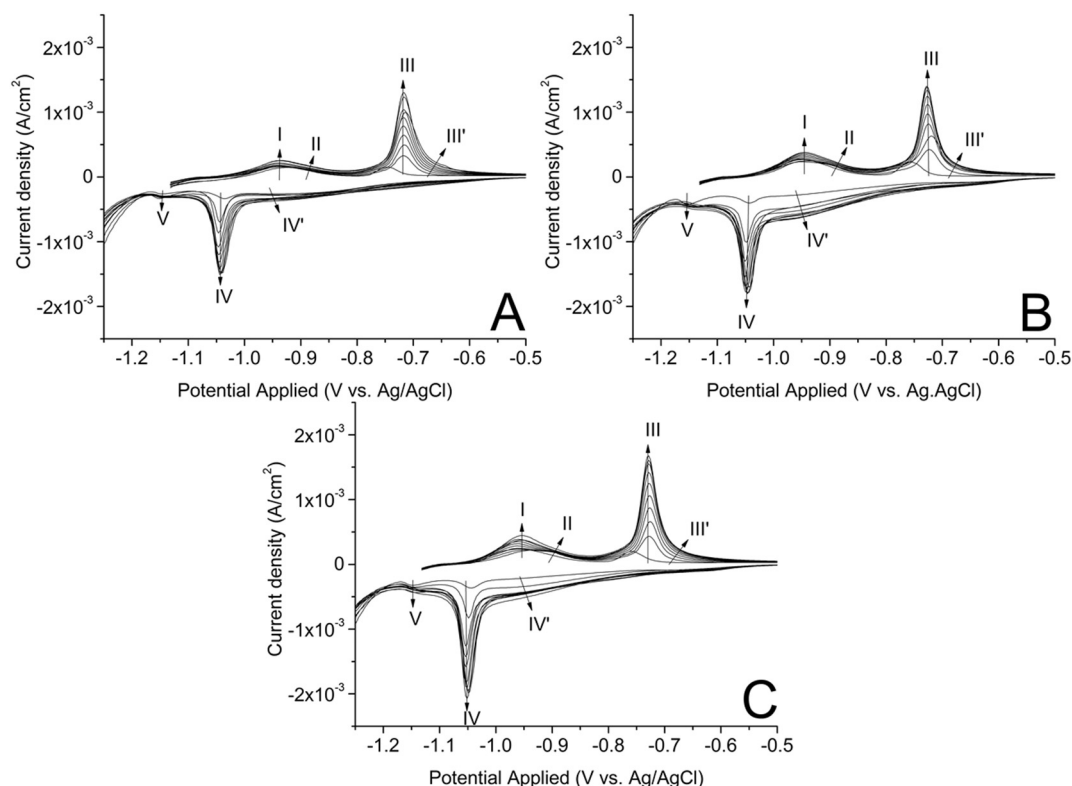


Fig. 1. Cyclic voltammograms of steel immersed in simulated pore solution with NaOH concentrations of: (A) 0.80 M (B) 1.12 M and (C) 1.36 M. Data were collected at a sweep rate of 2.5 mV/s. Arrows indicate the current response from scan numbers 1 to 10. Data from -1.50 V to -1.13 V in the anodic sweeps are not presented to enable visibility of peak V.

ions in the potential range of peak II in concentrated alkaline solutions where $\text{pH} > 14$. According to the Pourbaix diagram for iron in water [2], it is reasonable to assume the formation of HFeO_2^- as an intermediate product in highly alkaline solutions, as has been reported by several authors [38,41,44]. The subsequent hydrolysis of the intermediary species, as indicated in reaction (6), results in the formation of $\text{Fe}(\text{OH})_2$. Schrebler Guzmán et al. [41] also suggested the existence of a precipitation-dissolution equilibrium between $\text{Fe}(\text{OH})_2$, HFeO_2^- and FeO_2^- .

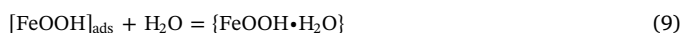
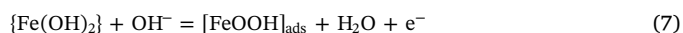
It is important to note here that several authors [37,45,46] have instead attributed peaks I and II to the formation of $\text{Fe}(\text{OH})_2$ and Fe_3O_4 respectively. However, the clear dependency of peaks I and II on the hydroxide concentration for the systems assessed in this study indicates that a dehydroxylation mechanism is highly unlikely to arise here. In the reverse sweeping direction, the broad cathodic current peak V can be assigned as the reduction couple of peaks I and II, indicating the reduction of the $\text{Fe}(\text{OH})_2$ to Fe^0 through the reversible mechanisms listed in reactions (3)–(6). This is supported by the fact that the sum of the anodic charges associated with current peaks I and II is approximately equal to the charge associated with current peak V, at all concentrations of OH^- . Similar observations have been reported by Schrebler Guzmán et al. [41].

In the case of anodic current peak III and cathodic current peak IV, repeated cycling led to an increase in the peak currents in both directions. Similar trends were observed for shoulders III' and IV'. After the first scan, anodic and cathodic current peaks III and IV shifted slightly towards more positive and negative potentials respectively, and occurred at relatively constant potentials during sweeps 2 to 10. The current densities of peaks III, III', IV and IV' increase with increasing NaOH concentration. Successive potential sweeps did not significantly alter the position or the current density of peak V. However, from being a distinct peak during the first scan, peak V changed into a less distinct and broader peak during subsequent sweeps. These observations are generally aligned with the literature describing the passivation

behaviour of steel in highly alkaline electrolytes [40,41].

The appearance of peak III indicates the oxidation of the Fe^{2+} species to a Fe^{3+} species [39]. The current density of peak III during potential sweeps is much higher than those of peaks I and II, and could possibly be related to the expansion of the structure of the passivation layer arising from the lower densities associated with Fe^{3+} species when compared to Fe^{2+} species [41]. The oxidation product formed during the anodic current peak III has been argued extensively in the literature to be various polymorphs of either FeOOH or Fe_2O_3 [37,38,47–49]. The anodic current density associated with peak III at about -0.72 V was observed to rise with increasing OH^- , and therefore the species formed at peak III due to the oxidation of $\text{Fe}(\text{OH})_2$ can be assigned to an iron species involving hydroxide. The anodic current contribution observed as shoulder III', located at the positive side of peak III, could possibly indicate the formation of a non-equilibrium species at peak III that undergoes either a structural transformation or a chemical change at shoulder III' to a more stable species.

Kabanov et al. [38] proposed that the passivation of iron is due to an adsorbed layer of FeOOH . However Schrebler Guzmán et al. [41] suggested that FeOOH transforms initially into $\text{Fe}_2\text{O}_3 \cdot \text{H}_2\text{O}$, and upon ageing takes on a structure similar to Fe_3O_4 or hydrated Fe_2O_3 . Similarly, Tschinkel et al. [48] assigned the oxidation product at peak III to be $\alpha\text{-FeOOH}$ or $\delta\text{-FeOOH}$ that later transformed into Fe_3O_4 . Considering the different observations by several authors in the literature, the following reactions (7), and then (8) or (9), could be possibly assigned to the anodic current peaks III and III' respectively:



It is evident that there still is no agreement in the literature on the oxidation reaction occurring at peaks III and III'. However, the formation of a hydrated oxide or oxy-hydroxide film that can undergo

chemical changes upon ageing seems to be a reasonable supposition.

In the reverse sweep, the cathodic current peaks IV and IV' can be directly assigned to the reduction couples of the oxidation reactions associated to peaks III and III' respectively. As seen from Fig. 1 the cathodic current contribution from peak IV is similar to that of the anodic current peak III, representing reduction of the Fe^{3+} species formed at peak III to $\text{Fe}(\text{OH})_2$. This is however not the case for the current contributions in shoulders IV' and III', and it is rather difficult to accurately characterise the location of IV'. Additionally, the current contribution in the forward sweep remains fairly constant at a relatively small non-zero value in the potential range -0.50 V to $+0.55$ V, which could possibly be due to further chemical changes in the oxidation product formed at peak III'. Therefore, on the reverse sweep, the cathodic contributions from the broad shoulder spanning from -0.50 V to -1.00 V could possibly represent the reduction of all the species formed in the forward sweep from -0.67 V (peak III') to 0.55 V. Cyclic voltammograms obtained with different sweep rates (5 mV/s and 10 mV/s, see Supporting information) were consistent with the results and interpretations presented here.

3.1.2. Open circuit potential, electrochemical impedance spectroscopy, linear polarisation resistance and anodic polarisation

OCP values measured at the start of the experiments were -0.30 V, -0.32 V and -0.32 V (± 15 mV) vs. Ag/AgCl for 0.80 M, 1.12 M and 1.36 M NaOH solutions respectively. According to the Pourbaix diagram [2], these potentials lie in the region where the steel is expected to be protected by a film containing Fe mainly as iron (III) oxides.

EIS was used to analyse the electrical properties of the passive film. Fig. 2 shows the Nyquist plot obtained for all three NaOH concentrations considered in this study, and the electrical equivalent circuit model used for fitting. From the Nyquist plots, a clear change in the electrochemical response of the system with decreasing frequency is evident. The spectra are characterised by an incomplete depressed semicircle at higher frequencies (10^4 Hz to 10^{-1} Hz), followed by a linear diffusion tail at lower frequencies (10^{-1} Hz to 10^{-2} Hz). Such behaviour is similar to that depicted by the classical Randles circuit [50], which was used to fit EIS data (Fig. 2). The equivalent circuit model was composed of:

- the electrolyte resistance (R_e),
- a constant phase element (CPE_{dl}) representing the imperfect capacitive nature of the double layer,
- a charge transfer resistance (R_{ct}) depicting the resistance of the passive film to charge transfer, and

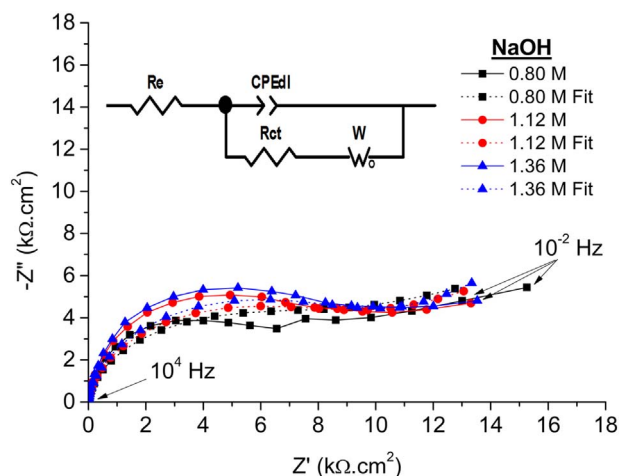


Fig. 2. Nyquist data and fitting plots for steel exposed to simulated pore solutions with varying NaOH concentrations. The equivalent circuit fitting model (modified Randles circuit) used to generate the fitting curve is also shown.

Table 3

Fitting results obtained for equivalent circuit model components related to EIS data shown in Fig. 2. All values are reported after surface area normalisation.

$[\text{OH}^-]$	R_e ($\Omega\text{-cm}^2$)	CPE_{dl} ($\mu\text{F}\text{-cm}^{-2}$)	α	R_{ct} ($\text{k}\Omega\text{-cm}^2$)	Y_o ($\mu\text{S}\text{s}^{-n}\text{-cm}^{-2}$)	χ^2
0.80 M	1.72	80.0	0.93	9.51	16.34	0.009
1.12 M	1.21	78.0	0.93	11.88	0.040	0.013
1.36 M	1.06	76.7	0.93	12.80	0.003	0.014

- a semi-infinite Warburg diffusion element (W_o) indicative of the mass transport processes occurring at the passive film/metal interface.

The use of a Warburg element in this model is related to the fact that the growth of the passive film on a metallic surface is primarily driven by the diffusion of oxygen vacancies from the solution/passive film interface to the passive film/metal interface [51,52]. Parameters in the high frequency region, R_e , R_{ct} and CPE_{dl} , were determined separately without the use of the Warburg element, primarily because of the underestimation of these parameters by the electrical equivalent circuit (shown in Fig. 2).

Table 3 shows the fitting parameters obtained for the electrical equivalent circuit model. The electrolyte resistance (R_e) was found to be between 1.72 and 1.06 $\Omega\text{-cm}^2$ for the three NaOH concentrations, and reduces at increased alkalinity and conductivities of the simulated pore solutions. The capacitance values of the CPE_{dl} element were almost independent of NaOH concentration, between 76 and 80 $\mu\text{F}\text{-cm}^{-2}$. The parameter α corresponds to CPE_{dl} , and the properties of the CPE are determined by the value of α ($0 \leq \alpha \leq 1$) [52]. When α is 1, the element is a capacitor, whereas the behaviour is governed by to diffusion/mass transfer when α approaches 0.50 [52]. The value of α in this study was 0.93 for all electrolyte concentrations, indicating the non-ideal but mainly capacitive nature of the solution/passive film interface. This deviation from ideal behaviour can be attributed to the non-homogeneous distribution of ions at the solution and the roughness of the electrode surface.

The resistance to charge transfer (R_{ct}) of the passive film increased from 9.51 to 12.80 $\text{k}\Omega\text{-cm}^2$ with a rise in $[\text{OH}^-]$. The admittance values (Y_o) associated with semi-infinite diffusion processes at the passive film/metal interface decreased from 16.34 to 0.003 $\mu\text{S}\text{s}^{-n}\text{-cm}^{-2}$, with increasing $[\text{OH}^-]$. Higher admittance values indicate an increased mass transport through the film, as it is directly related to the diffusivity of ionic species through the film [53]. Such trends in R_{ct} and Y_o can be attributed to the existence of a directly proportional relationship between the concentration of hydroxide in the electrolyte and the protective nature of the passive film. Therefore, a rise in the R_{ct} value, and consequently reduction in Y_o value, with increasing alkalinity, is associated with an increased concentration of passivating species on the surface of the electrode.

The Nyquist plots (Fig. 2) present a non-conventional nature of the diffusion tail, where at low frequencies the slope between the imaginary and real components of impedance was much lower than 45° . This indicates a slow transition from the capacitive behaviour of the solution passive/film interface to the diffusional behaviour of the passive film/metal interface, and could be a result of the mass transfer resistance of the passive film and the consequentially low diffusivity of ions through the passive film. Therefore, if the frequency domain used in this study was extended to even lower frequencies, the appearance of a conventional diffusional tail would be anticipated.

R_p values calculated from linear polarisation measurements were analogous to the trend for R_{ct} observed through EIS, and were found to be 45.5, 67.6 and 88.2 $\text{k}\Omega\text{-cm}^2$ for 0.80 M, 1.12 M and 1.36 M NaOH solutions, respectively.

Anodic polarisation curves obtained for the three NaOH

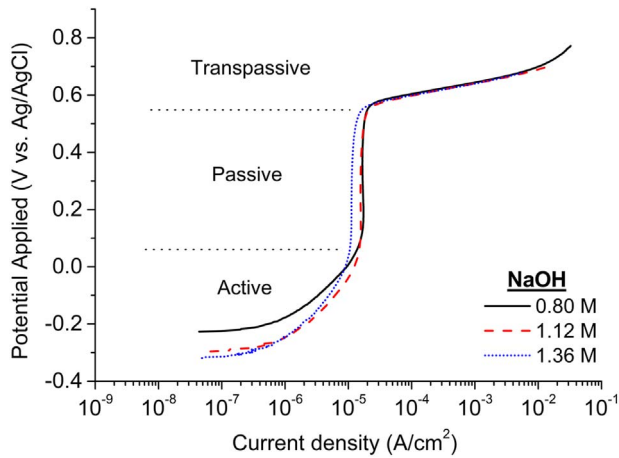


Fig. 3. Anodic polarisation curves obtained for steel rebars immersed in chloride-free simulated pore solutions, as a function of the NaOH concentration.

concentrations are shown in Fig. 3. All three polarisation curves follow the same trend with clearly defined active, passive and trans-passive regions. On increasing the potential in the positive direction from the OCP, the current density was observed to increase steadily until the potential reaches about 0.10 V, representing the active region where the electrode surface reacts with the electrolyte to form a passive film. The current density remained fairly constant when the potential was increased from 0.10 V to about 0.55 V, indicating the steel (electrode) being protected against corrosion by the passive film. A sharp rise in the current density was evidenced when the potential was increased from 0.55 V onwards, typical of the oxygen evolution reaction.

The current densities recorded in the passive region decreased with increasing $[OH^-]$ in the electrolyte, indicating a direct relationship between the degree of passivation and the alkalinity of the solution. This is consistent with EIS and LPR measurements, where an increased alkalinity results in a higher resistance and a reduction in the admittance of the passive film.

3.2. Depassivation

3.2.1. Open circuit potential

Fig. 4 shows the measured open circuit potentials for steel immersed in simulated pore solutions with different concentrations of hydroxide (0.80, 1.12 and 1.36 M) and chlorides. In the case of 0.80 M NaOH solutions, the steel rebars (working electrode) exhibited fairly constant

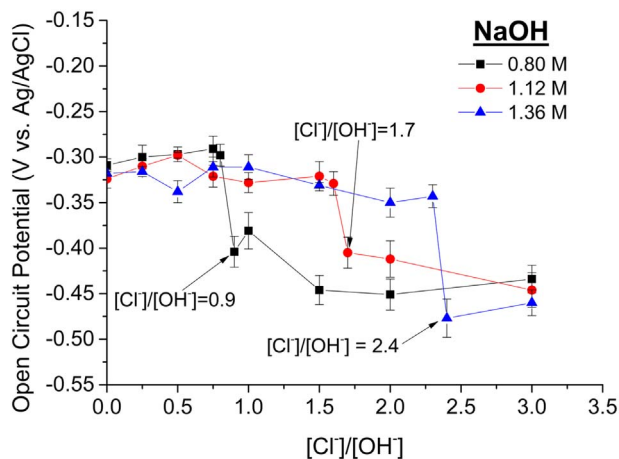


Fig. 4. Measured open circuit potential values (V vs. Ag/AgCl) for steel immersed in chloride-contaminated NaOH solutions. OCP values are plotted against the ratio $[Cl^-]/[OH^-]$.

OCP values for chloride additions from zero up to 0.64 M, followed by a sudden drop in the potential for chloride concentrations > 0.64 M. A similar trend was observed for 1.12 M and 1.36 M NaOH solutions, where the sudden drop in OCP values was identified at chloride concentrations > 1.79 M and 3.13 M, respectively. In terms of $[Cl^-]/[OH^-]$ ratios, the sharp decrease in OCP was observed when the ratio $[Cl^-]/[OH^-]$ was > 0.80 , 1.60 and 2.30 for 0.80 M, 1.12 M and 1.36 M NaOH solutions respectively.

All the OCP values shown Fig. 4 lie in the range of potential values where the steel is protected by a passive film [2], with a complex chemical and phase composition that includes species containing iron in (II) and (III) oxidation states. However, the notable reduction in the potentials at particular concentrations of chloride (which are different for each $[OH^-]$) indicates the interaction of chloride with the passive film.

From the OCP values, it is possible to conclude that depassivation of the steel does not occur until the chloride concentration reaches a critical value (C_{crit} or $[Cl^-]/[OH^-]$ ratio) which is directly dependent on the amount of hydroxide present in the vicinity of the electrode surface. The C_{crit} value (in terms of chloride concentration) for the assessed steel immersed in a 1.36 M NaOH was approximately 1.91 and 3.62 times higher than that detected in rebars immersed in 1.12 M and 0.80 M NaOH solutions respectively. In terms of $[Cl^-]/[OH^-]$ ratios, the above C_{crit} values can be represented as 0.90, 1.70 and 2.40, for 0.80 M, 1.12 M and 1.36 M NaOH solutions respectively. This result is consistent with earlier observations indicating a rise in C_{crit} with an increase in the pH of the electrolyte [8,11,14,54]. This relationship will be revisited below, with input also from additional characterisation methods to provide deeper insight into the factors which control C_{crit} .

3.2.2. Linear polarisation resistance

Fig. 5 shows the polarisation resistance (R_p) values obtained via LPR analysis, as a function of the $[Cl^-]/[OH^-]$ ratio. R_p values were determined from the slope of the voltage vs. current plot obtained by varying the potential from -20 to $+20$ mV vs. OCP. The R_p values of the steel exhibited a sharp decrease when the chloride concentration was equivalent to the same $[Cl^-]/[OH^-]$ (C_{crit}) ratios of 0.90, 1.70 and 2.40 determined via OCP analysis (Fig. 4), for 0.80 M, 1.12 M and 1.36 M NaOH solutions, respectively. The findings from LPR clearly demonstrate that the passive film on the steel surface remains intact until the chloride concentration reaches a critical value to induce depassivation. This critical value of chloride required for depassivation depends strongly on the hydroxide concentration in the pore solution. Ghods et al. [54] reported a similar trend in R_p values when investigating chloride induced depassivation of black steel reinforcement.

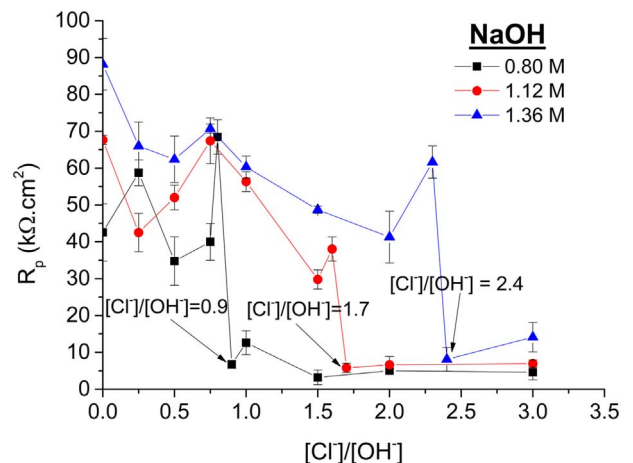


Fig. 5. Linear polarisation resistance measurements for steel rebars immersed simulated pore solutions with different concentrations of NaOH, as a function of the $[Cl^-]/[OH^-]$ ratios.

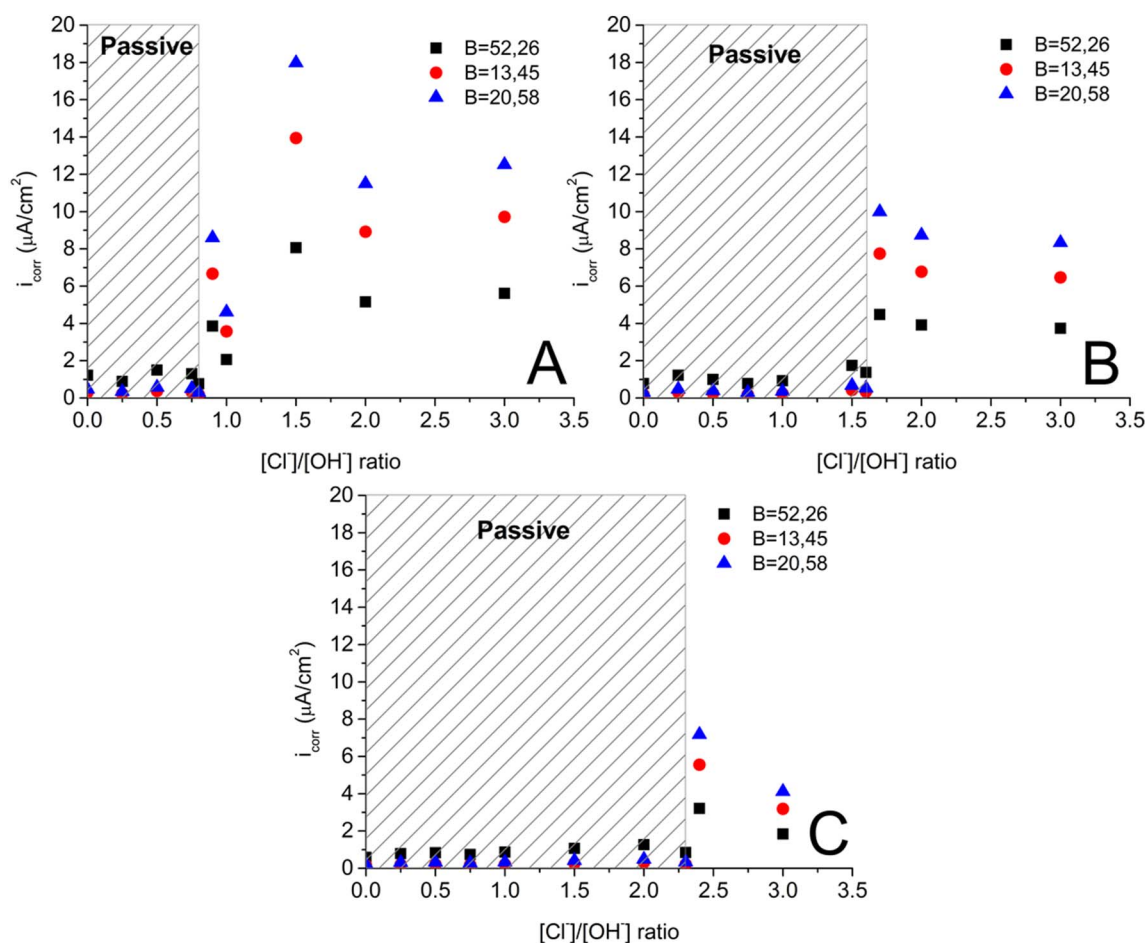


Fig. 6. Variations of i_{corr} ($\mu\text{A}/\text{cm}^2$) of steel rebars immersed in simulated pore solutions with a $[\text{NaOH}]$ of (A) 0.80 M, (B) 1.12 M and (C) 1.36 M, as a function of $[\text{Cl}^-]/[\text{OH}^-]$ ratio. Legend entries represent the values of B used in the Stern-Geary equation for active and passive samples: $B = i_j$; where $i =$ value of B for passive samples, and $j =$ value of B for active samples. B values are taken from [34,36]. Shaded regions show the region where the steel is in a passive state.

Corrosion current densities (i_{corr}) were calculated using the Stern-Geary relationship (Eq. (2)) and are shown in Fig. 6, as a function of $[\text{Cl}^-]/[\text{OH}^-]$ ratio. Corrosion rate determinations in reinforced PC concretes generally use 26 mV and 52 mV as the values of the proportionality constant ‘ B ’ for active and passive samples, respectively [36]. The applicability of the aforementioned ‘ B ’ values for reinforced low-Ca alkali-activated concretes was assessed by Babae and Castel [34], and the appropriate proportionality constants for these materials were found to diverge significantly from these values. They found that B was between 13 mV and 20 mV for passive alkali-activated samples, and between 45 mV and 58 mV for active samples. Three sets of i_{corr} values were thus calculated in this study, using the B values suggested by Andrade et al. [36], and the lower and upper limits from the work of Babae and Castel [34]. As seen in Fig. 6, sudden changes in the i_{corr} values are observed for the three pore solutions when the chloride concentration reaches the same $[\text{Cl}^-]/[\text{OH}^-]$ (C_{crit}) ratios defined through OCP and R_p measurements, and accordingly the active and passive conditions of steel as a function of chloride concentration can be defined.

When the steel is in its passive state, the i_{corr} values remain fairly constant for each set of B values, and are lower for solutions with increased alkalinity, consistent with the higher degree of passivation of steel in pore solutions with higher $[\text{OH}^-]$. In comparison to the current density of $0.1 \mu\text{A}/\text{cm}^2$ or lower, proposed by Andrade et al. [36] as the criterion for steel to exhibit a passive nature in PC concretes, the calculated i_{corr} values in this study for steel in the passive state are 5–10 times higher when using the value of B from [36], and 2–3 times higher when the value of B is taken according to [34]. Even though the i_{corr}

values in the passive region are much higher than $0.1 \mu\text{A}/\text{cm}^2$, no active corrosion was observed for chloride concentrations less than the respective $[\text{Cl}^-]/[\text{OH}^-]$ (C_{crit}) ratios for these solutions. The differences in the i_{corr} values can be attributed to several possible reasons, including the measurements being conducted in simulated pore solutions rather than concrete specimens, and the differences in the chemistry and alkalinity of the simulated pore solutions for low-Ca alkali-activated binders compared to PC.

When the concentration of chloride is higher than C_{crit} for different pore solutions, the values of i_{corr} are much higher when compared to those in the passive region, indicative of active pitting corrosion. The observations of lower corrosion current densities for solutions with increased alkalinity were also true for the active corrosion region (Fig. 6). In contrast to the situation for the passive region, the corrosion current densities of steel calculated using the B values accepted for PC systems in the active region are much lower when compared to those proposed for low-Ca alkali-activated binders.

3.2.3. Anodic polarisation

Fig. 7 shows anodic polarisation curves obtained for steel rebars immersed solutions with varying concentrations of NaOH and chloride. In all three NaOH concentrations, the anodic polarisation curves were similar to that observed for steel in its passive state (Fig. 3) until chloride concentrations in each electrolyte reaches the corresponding C_{crit} values identified in Sections 3.2.1 and 3.2.2. Such an observation clearly complements the conclusions from OCP and LPR measurements, and signifies the fact that depassivation of steel does not initiate unless the concentration of chloride reaches a critical value, which is strongly

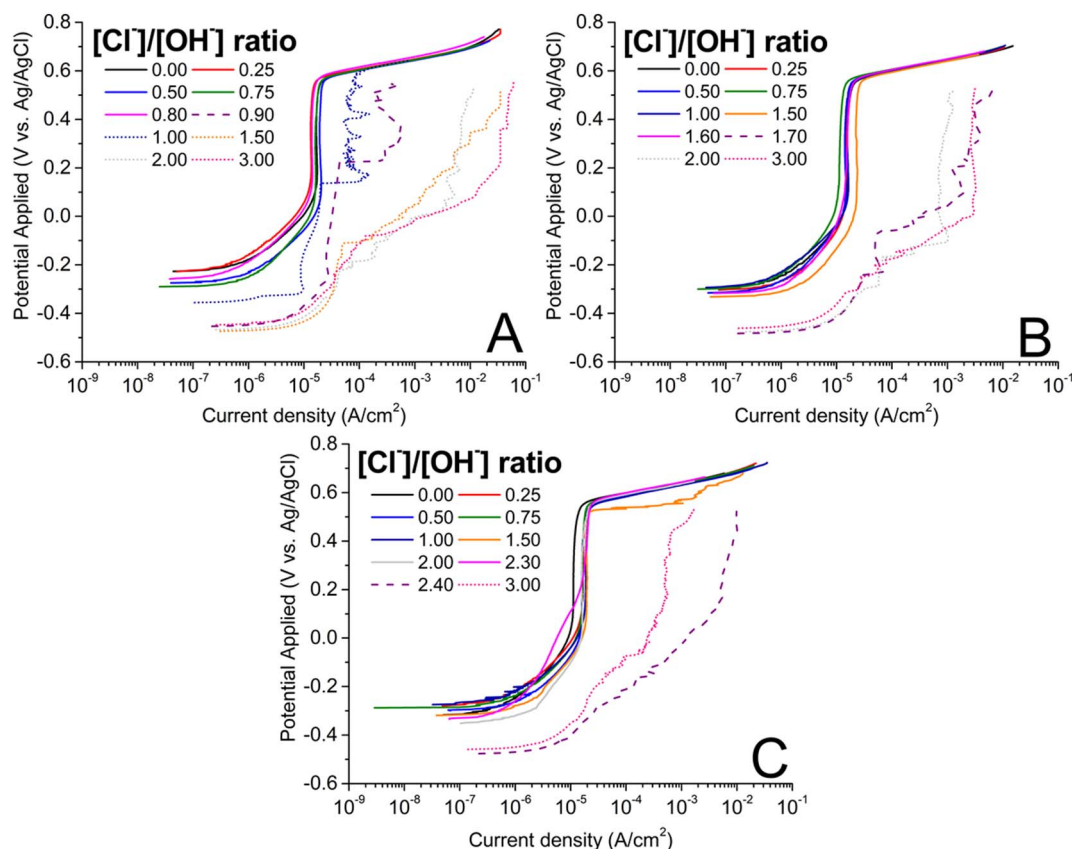


Fig. 7. Anodic polarisation curves obtained for steel immersed in (A) 0.80 M, (B) 1.12 M and (C) 1.36 M NaOH solutions with varying concentrations of chloride. Solid lines (—) represent data for passive samples, dashed lines (- -) represent data for respective chloride threshold values and dotted lines (····) represent data for chloride concentrations above the chloride threshold value.

correlated to the alkalinity of the pore solution. Upon reaching the C_{crit} concentrations for different pore solutions, the anodic polarisation curves presented a smaller or an absent passivation region. Instead, on attaining specific anodic potentials (the pitting potential, E_{pit}), abrupt increases in the current densities were observed, indicative of either pit nucleation, metastable pitting, or stable pit growth.

It could be reasonably expected that an increase in the concentration of chloride higher than C_{crit} would result in increased current densities. This is not the case in all three NaOH concentrations, primarily because of the number of variables (e.g. microstructure and surface features of different steel specimens, the presence of defects and inclusions, and the location of pitting) and the local chemistry of the pore solution around the pit) associated with pitting. Therefore, the current densities observed in the anodic polarisation curves cannot be used as the sole determining factor in quantitatively ranking the degree of pitting corrosion for various steel specimens in the presence of an aggressive species. However, anodic polarisation can be successfully employed to predict the chloride concentration required for initiation of depassivation and stable pit growth.

Chloride induced corrosion initiates through the localised breakdown of the passive film (more likely at grain boundaries, or defect sites) and propagates by the nucleation and growth of pits [55,56]. The breakdown of the passive film at highly localised sites only occurs when the local concentration of chloride reaches a critical value, leading to the formation of a pit. Once a pit nucleates, pit growth is only possible when the solution in the pit cavity maintains an aggressive environment compared to the bulk electrolyte surrounding it [57]. To fulfil this requirement, a sustained anodic dissolution of iron and subsequent hydrolysis of iron ions to form H^+ inside the pit cavity is essential [58]. Such a process decreases the relative alkalinity inside the pit cavity and leads to the growth of pits. The process of stable pit growth ceases when

the anions in the surrounding environment, such as OH^- , migrate into the pit cavity to maintain charge neutrality, resulting in the re-passivation of the steel surface [57,59]. The migration of anions into the pit cavity is directly dependent on the local availability/reservoir of anions and the pit geometry. The mechanism by which some of the nucleated pits fail to achieve stability and re-passivate due to the surrounding chemistry has been termed ‘metastable pitting’ [57].

When the ratio $[Cl^-]/[OH^-]$ was either 0.90 or 1.00 in 0.80 M NaOH solution (Fig. 7A), apparently random fluctuations (increments and decrements) in the current density were observed as the potential increased from 0.22 V or 0.13 V respectively. Given the high alkalinity in the electrolytes used in this study, and that this behaviour is only observed at chloride concentrations close to C_{crit} , this phenomenon can be explained by the formation of metastable pits. Therefore, it could be concluded that the amount of chloride required to initiate pit nucleation may not necessarily be the same that is required for stable pit growth. For the same electrolyte, stable pitting was observed for $[Cl^-]/[OH^-]$ ratios above 1.00.

From the anodic polarisation curves for steel immersed in 1.12 M (Fig. 7B) and 1.36 M (Fig. 7C) NaOH solutions, distinct transitions from the passive condition to metastable pitting to stable pit growth is not observed for the concentrations of chloride tested. However, it could be assumed that such a transition occurs at some $[Cl^-]/[OH^-]$ ratio lying between 1.60 and 1.70 when the concentration of $[OH^-]$ is 1.12 M, and between 2.30 and 2.40 when the $[OH^-]$ concentration is 1.36 M.

Similar observations of repassivation have been reported [20,57,60,61] for steel embedded in PC concrete, as well as immersed in simulated pore solutions representative of PC systems. PC binders are characterised by the formation of large amounts of portlandite ($Ca(OH)_2$) during the hydration of calcium silicates [28]. Portlandite present at the steel-concrete interface plays an important role in

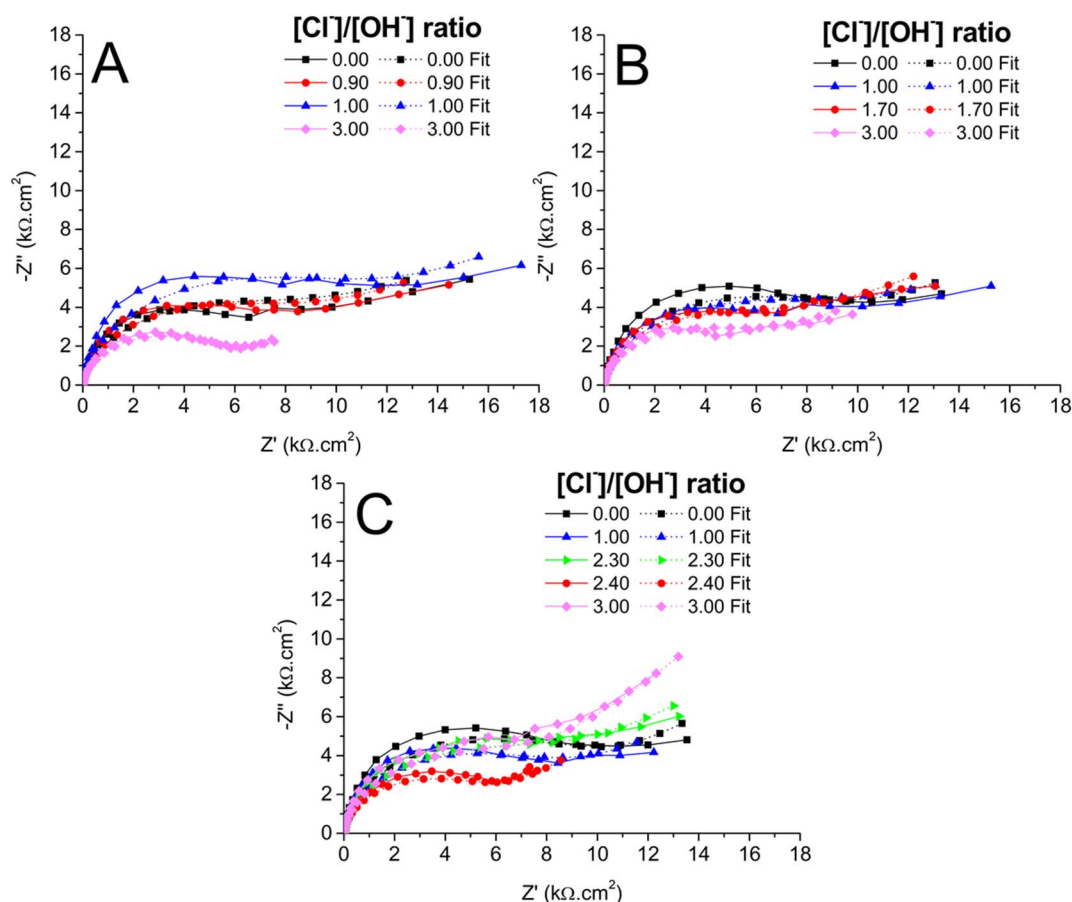


Fig. 8. Nyquist data and fitting plots for steel exposed to (A) 0.80 M, (B) 1.12 M and (C) 1.36 M NaOH solutions with varying chloride concentrations. Solid lines such as —●— represents the impedance data obtained for respective chloride threshold values, and dashed lines with the same markers, e.g. -●-, represent the corresponding fits.

Table 4

Fitting results obtained for equivalent circuit model components relating to EIS data shown in Fig. 8.

$\frac{[\text{Cl}^-]}{[\text{OH}^-]}$	R_e ($\Omega\text{-cm}^2$)	CPE_{dl} ($\mu\text{F}\text{-cm}^{-2}$)	α	R_{ct} ($\text{k}\Omega\text{-cm}^2$)	Y_0 ($\mu\text{S}\text{-s}^n\text{-cm}^{-2}$)	χ^2
0.80 M NaOH						
0.00	1.72	80.0	0.93	9.5	16.3	0.009
0.90	1.43	75.9	0.93	9.5	85.9	0.008
1.00	1.40	72.2	0.93	12.8	263.7	0.013
3.00	0.95	89.4	0.93	6.0	5420	0.002
1.12 M NaOH						
0.00	1.21	78.0	0.93	11.9	0.04	0.013
1.00	1.00	76.4	0.93	8.9	0.03	0.007
1.70	0.93	73.8	0.93	8.6	46.3	0.006
3.00	0.91	95.4	0.93	6.5	4350	0.005
1.36 M NaOH						
0.00	1.06	76.7	0.93	12.8	0.003	0.014
1.00	1.02	92.7	0.93	9.9	0.002	0.011
2.30	0.95	87.5	0.92	10.9	0.004	0.006
2.40	0.98	91.7	0.92	7.0	62.07	0.005
3.00	0.96	80.5	0.92	10.7	3248	0.008

determining the mechanism of corrosion initiation of the embedded steel, as it acts as a reservoir of soluble Ca^{2+} and OH^- ions [28]. The dissolution of portlandite around the pit nucleation site acts as a buffer ensuring sufficient availability of $[\text{OH}^-]$ to neutralise the aggressive environment in the pit cavity, resulting in repassivation of the pit. Once the local reservoir of portlandite has been exhausted, stable pit growth will occur. However, unlike PC binders, low-Ca AAMs do not contain any observable portlandite that could provide a buffer effect, meaning

that repassivation of a nucleated pit in such systems will primarily be influenced by other factors such as the diffusivity of hydroxide ions from the bulk solution.

3.2.4. Electrochemical impedance spectroscopy

Fig. 8 shows the Nyquist data and fitting plots obtained for steel specimens immersed in solutions with varying concentrations of NaOH and chloride. Based on the OCP and LPR measurements, EIS analysis was conducted on steel exposed to selected concentrations of chloride (with $[\text{Cl}^-]/[\text{OH}^-]$ ratios = 0, 1.00, 3.00 and their corresponding C_{crit} values). The equivalent circuit model used was similar to the classical Randles circuit, as shown in Fig. 2. As discussed in Section 3.1.2, pitting corrosion is primarily driven by the diffusion of anionic species inside and outside the pit cavity, so the use of a Warburg diffusion element is justified. However, as in the analysis of passivation discussed in Section 3.1.2, the high frequency regions were characterised separately without the Warburg element.

Upon the introduction of chloride, the general characteristics of the Nyquist plots did not change significantly when compared to steel in passivated conditions, where the higher frequencies reflected the non-ideal capacitive nature of the solution/passive film interface, and the lower frequencies showed a linear diffusion tail representing semi-infinite diffusion at the passive film/metal interface. Table 4 shows the fitting parameters obtained for the equivalent circuit model described earlier, in the presence of chloride.

With increasing ionic strength or increasing chloride concentrations, the electrolyte resistance (R_e) decreases; this was consistent for all the three NaOH concentrations assessed. The capacitance associated with the CPE_{dl} varied between 72 and $95 \mu\text{F}\text{-cm}^{-2}$ and the value of α was constant at 0.93 ± 0.01 for all solutions, demonstrating minimal

changes of the double layer at the solution/passive film interface. The charge transfer resistance of the passive film (R_{ct}) did not exhibit any specific trend with increasing chloride concentrations for all the pore solutions; however, the values are consistent with the observations of anodic polarisation.

As seen in Fig. 7A for 0.80 M NaOH, the current density was much higher for a $[Cl^-]/[OH^-]$ ratio of 0.90 than 1.00. Correspondingly, the R_{ct} values mentioned in Table 4 were lower for $[Cl^-]/[OH^-]$ ratio of 0.90, than for $[Cl^-]/[OH^-] = 1.00$. Similar correlations between measured R_{ct} values obtained through EIS and current density determined through anodic polarisation could be made in the case of 1.36 M NaOH solutions, when the $[Cl^-]/[OH^-]$ ratios were 2.40 and 3.00. It is important to mention that, although the timescales allowed in this study for the passive film to stabilise in the simulated pore solutions were much less than that suggested by other studies [54,62,63], the chemical nature of the film could be considered to be representative of what would exist after the suggested stabilisation timescales but with a lesser thickness. As shown by several authors [45,52], both the R_{ct} and CPE_{dl} parameters of the passive film are related to the time of exposure and are somewhat dependent on its physical nature. Therefore, variation in the values of R_{ct} and CPE_{dl} could be expected at longer times of exposure, but the electrical properties of the system would remain unaffected.

A substantial rise in the admittance (Y_0), characterising diffusion at the passive film/metal interface, was observed when the chloride concentration exceeded the respective C_{crit} values for the three pore solutions. As in the EIS study of passivation discussed in Section 3.1.2, non-conventional diffusion tails in the low frequency region were also observed upon addition of chloride, for all three NaOH concentrations. However, the slope between the real and imaginary components of impedance at lower frequencies approached its conventional slope of 45° for all $[Cl^-]/[OH^-]$ ratios where the steel specimens underwent pitting.

The admittance can be physically interpreted as the ease of transport of chloride ions through the passive film to the metal, and it is described as a function of the stability of the passive film. When the concentration of chloride is lower than C_{crit} , the steel is maintained in its passive state and consequently the admittance is fairly constant at a relatively low value, similar to that observed for chloride-free solutions. Hence, the diffusion of ions through the passive film to the metal surface can be considered to be not rapid enough to be detected at frequencies as low as 10^{-2} Hz, leading to the non-conventional diffusion tail. A breakdown of the passive film by the action of chloride would lead to easier transport of ions and a rise in the admittance value (Table 4). Thus, on increasing the chloride concentrations to C_{crit} and above, the diffusivity associated with the passive film would significantly increase due to the action of chloride on the passive film, and would lead the slope between real and imaginary components of impedance to approach 45° .

3.3. Observations on passivation and the chloride threshold value

Several relationships between C_{crit} and $[OH^-]$ have been reported in studies conducted in simulated concrete pore solutions. Hausmann [64] experimentally reported the value of $[Cl^-]/[OH^-]$ ratio to vary between 0.5 and 1.08, and statistically found the ratio of 0.63 as critical. Gouda [8] suggested a linear relationship between pH and the logarithm of the critical chloride concentration with a slope of 0.83, implying a constant value of $[Cl^-]^{0.83}/[OH^-]$. Goni and Andrade [12] found a linear relationship between the logarithm of corrosion current density and the logarithm of $[Cl^-]/[OH^-]$ ratios, and on assuming the boundary condition for active corrosion in the range of 0.1–0.2 $\mu A/cm^2$ suggested a threshold value between 0.25 and 0.8. Similar observations have been made in other studies including [11,15], where the critical chloride content for depassivation were witnessed to increase with higher pH.

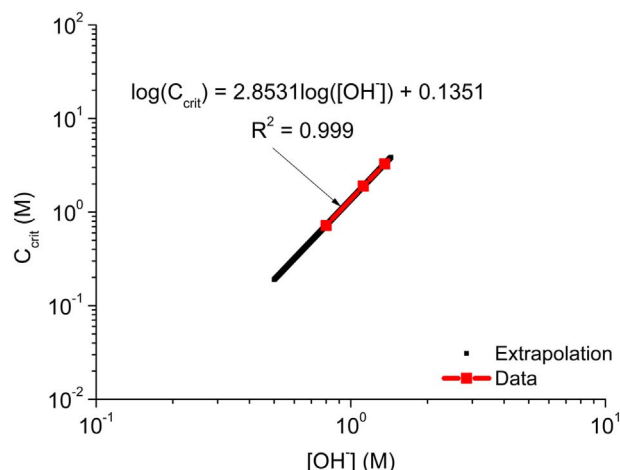


Fig. 9. Relationship between C_{crit} and $[OH^-]$. Red points and the regression equation correspond to the experimental data. Black points represent extrapolated values. (For interpretation of the references to colour in this figure legend, the reader is referred to the web version of this article.)

Measurements from all of the techniques used in this study to analyse chloride induced depassivation of the steel in simulated pore solutions representative of low-Ca AAMs, confirm a strong correlation between the concentration of hydroxide and the chloride threshold value. The C_{crit} values were found to be 0.72 M, 1.90 M and 3.26 M for pore solutions with $[OH^-]$ concentrations of 0.80 M, 1.12 M and 1.36 M respectively. Contrary to the observation of diverging C_{crit} values for a particular electrolyte obtained through different techniques in [54], here we identify the same C_{crit} value through several electrochemical techniques for a given electrolyte.

To develop a relationship between the measured C_{crit} values and the $[OH^-]$ concentration of the simulated pore solution, C_{crit} values were plotted against $[OH^-]$, as shown in Fig. 9. A linear correlation between the logarithm of C_{crit} and logarithm of $[OH^-]$ with a slope of 2.83 was fitted, implying an increased inhibition effect with an increase in $[OH^-]$. Given the heterogeneous nature of the steel-concrete interface (generally due to macroscopic and microscopic voids, varying hydration products and pore solution alkalinity, bleed-water zones) and the possible carbonation of pore solution, the derived relationship was used to extrapolate for values of $[OH^-]$ ranging between 0.5 and 1.43 M. The C_{crit} values obtained through the above-mentioned extrapolation method (as shown in Fig. 9) show that even a chloride concentration as low as about 0.18 M, in regions at the steel-concrete interface where $[OH^-]$ is 0.5 M, could possibly initiate pitting of the embedded steel rebar. Here it is important to highlight that this relationship may be valid only when the binder does not contain any alkaline buffering agent (such as portlandite in PC-based concretes), as in low-Ca AAMs. For example, if the relationship was extrapolated to pH 13, or an OH^- concentration of 0.1 M, the resulting C_{crit} would be around 10^{-3} M. This would differ significantly from the C_{crit} values reported in the literature (as reviewed by Angst et al. [10]).

The localised phenomena of depassivation by the action of chloride is primarily governed by the dissolution of the passive film, and therefore it can be hypothesised that the onset of pitting would be directly proportional to the concentration of chloride and inversely related to the solubility of the passive film for a particular electrolyte. For a given composition of the passive film, all electrochemical parameters should reflect the onset of pitting at a similar value of $[Cl^-]/[OH^-]^n$, where n is the stoichiometric coefficient of $[OH^-]$ in the hydrated outer layer of the passive film. According to the results of cyclic voltammetry in Section 3.1.1, the passive film is composed of an outer layer of hydrated $FeOOH$ or Fe_2O_3 for all three electrolytes. Therefore, considering a monohydrate layer of $Fe(OH)_3$ as the outer layer of the passive film, the value of n could be taken to be 3; this value is also the nearest

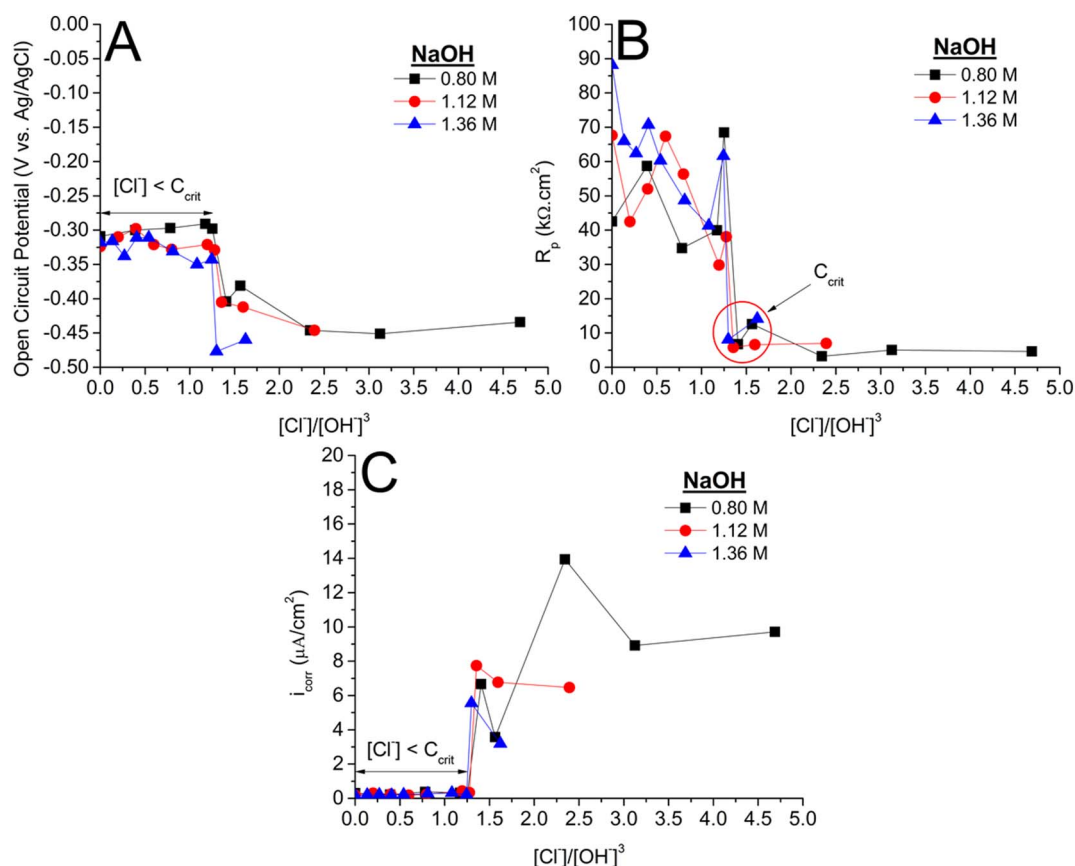


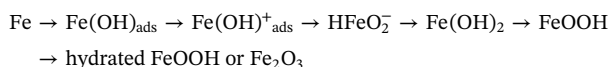
Fig. 10. Representation of (A) OCP, (B) R_p and (C) i_{corr} as a function of $[Cl^-]/[OH^-]^3$, for steel rebars immersed in simulated pore solutions with varying NaOH concentrations.

integer value to the 2.85 fitted above.

Fig. 10 shows the variation of different electrochemical parameters (OCP, R_p and i_{corr}) as a function of the ratio $[Cl^-]/[OH^-]^3$, for all three pore solutions assessed. The three parameters OCP, R_p and i_{corr} were observed to be close to constant for $0 \leq [Cl^-]/[OH^-]^3 \leq 1.25$; these values of $[Cl^-]/[OH^-]^3$ correspond to chloride concentrations less than the measured C_{crit} values for the three pore solutions, and thus not high enough to cause depassivation. Above the value of $[Cl^-]/[OH^-]^3 = 1.25$, OCP and R_p showed a sharp decline whereas i_{corr} values increased suddenly, indicating active corrosion. The sharp transition from the passive to the active region was found to occur very close to $[Cl^-]/[OH^-]^3 = 1.25$ for all three pore solutions, and the respective C_{crit} values aligned at this value. This confirms the existence of a hydrated $FeOOH$ or Fe_2O_3 as the outer layer of the passive film on all the steel specimens tested. The relationship thus appears to provide a powerful and novel means of characterising the likely onset of steel corrosion in low-calcium alkali-activated binders, at least as far as can be predicted through experimental work in simulated pore solutions.

4. Conclusions

It is demonstrated through the analysis of the anodic and cathodic current peaks from cyclic voltammetry, that in highly alkaline solutions the mechanism of passive film formation can be described as:



This implies that the passive film is composed of an inner dense layer rich in iron (II) species and the outer layer is rich in a less dense iron (III) species. The amounts of passivating species formed on the surface of the steel specimen are directly proportional to the alkalinity

of the solution. This is consistent with results of EIS, LPR and anodic polarisation, revealing a higher degree of the passivation at increased concentrations of OH^- in the pore solution.

The C_{crit} values (in terms of $[Cl^-]/[OH^-]^3$) obtained from OCP, EIS, LPR and anodic polarisation are comparable and within 0.90 ± 0.10 , 1.70 ± 0.10 and 2.40 ± 0.10 for NaOH concentrations of 0.80 M, 1.12 M and 1.36 M, respectively. It is clearly seen that an increased concentration of OH^- in the system, results in a rise in the chloride threshold value, as a consequence of improved passivation of the steel. Given the high alkalinity of the simulated pore solutions representative of low-Ca alkali-activated binders, the amounts of chloride at the steel-concrete interface required for pit nucleation and the amounts required for sustained pit growth might differ, and this led to observations of metastable pitting in some cases.

A novel relationship of depicting the onset of pitting as a function of the composition of the outer layer of the passive film, in terms of the ratio $[Cl^-]/[OH^-]^3$ was developed, where $[Cl^-]/[OH^-]^3 = 1.25$ was found to define the critical chloride concentration C_{crit} within the very highly alkaline range of solutions assessed. Rather than the simple ratio between chloride and hydroxide concentrations that is often used to define C_{crit} , this power law relationship provides improved descriptive power for solutions representative of the pore solution chemistry of low-calcium alkali-activated binders. The functional form used, with a third power relationship to hydroxide concentration, is also consistent with the passive film being composed of a hydrated $FeOOH$ or Fe_2O_3 outer layer that plays an important part in the initiation of pitting corrosion. However, further research related to different passivation products needs to be done to confirm such a relationship for pit initiation, and particularly to understand its validity in actual concrete specimens, and also in pore solutions which are not as extremely alkaline as those studied here.

Acknowledgements

The research leading to these results received funding from the European Research Council under the European Union's Seventh Framework Programme (FP/2007–2013)/ERC Grant Agreement #335928. The authors would like to acknowledge the technical support provided by Dr Oday Hussein. The authors would also like to thank Mr Kieran Nash from the Department of Civil and Structural Engineering at The University of Sheffield for providing the rebars.

Appendix A. Supplementary cyclic voltammetry data

Supplementary data to this article can be found online at <http://dx.doi.org/10.1016/j.cemconres.2017.08.006>.

References

- [1] M. Pourbaix, Thermodynamics and corrosion, *Corros. Sci.* 30 (1990) 963–988.
- [2] M. Pourbaix, Lectures on Electrochemical Corrosion, Springer Science & Business Media, 1973.
- [3] M. Pourbaix, Applications of electrochemistry in corrosion science and in practice, *Corros. Sci.* 14 (1974) 25–82.
- [4] K.K. Sagoe-Grentsil, F.P. Glasser, Steel in concrete: part II electron microscopy analysis, *Mag. Concr. Res.* 41 (1989) 213–220.
- [5] S. Haupt, H.H. Strehlow, Corrosion, layer formation, and oxide reduction of passive iron in alkaline solution: a combined electrochemical and surface analytical study, *Langmuir* 3 (1987) 873–885.
- [6] P. Ghods, O.B. Isgor, J.R. Brown, F. Bensebaa, D. Kingston, XPS depth profiling study on the passive oxide film of carbon steel in saturated calcium hydroxide solution and the effect of chloride on the film properties, *Appl. Surf. Sci.* 257 (2011) 4669–4677.
- [7] S. Joiret, M. Keddad, X.R. Nóvoa, M.C. Pérez, C. Rangel, H. Takenouti, Use of EIS, ring-disk electrode, EQCM and raman spectroscopy to study the film of oxides formed on iron in 1 M NaOH, *Cem. Concr. Compos.* 24 (2002) 7–15.
- [8] V.K. Gouda, Corrosion and corrosion inhibition of reinforcing steel: I. immersed in alkaline solutions, *Br. Corros. J.* 5 (1970) 198–203.
- [9] V.K. Gouda, W.Y. Halaka, Corrosion and corrosion inhibition of reinforcing steel: II. embedded in concrete, *Br. Corros. J.* 5 (1970) 204–208.
- [10] U. Angst, B. Elsener, C.K. Larsen, Ø. Vennesland, Critical chloride content in reinforced concrete - a review, *Cem. Concr. Res.* 39 (2009) 1122–1138.
- [11] L. Li, A.A. Sagues, Chloride corrosion threshold of reinforcing steel in alkaline solutions - open-circuit immersion tests, *Corrosion* 57 (2001) 19–28.
- [12] S. Goñi, C. Andrade, Synthetic concrete pore solution chemistry and rebar corrosion rate in the presence of chlorides, *Cem. Concr. Res.* 20 (1990) 525–539.
- [13] K. Pettersson, Corrosion threshold value and corrosion rate in reinforced concrete, *CBI Rep.* 292 (1992).
- [14] L.T. Mammoliti, L.C. Brown, C.M. Hansson, B.B. Hope, The influence of surface finish of reinforcing steel and pH of the test solution on the chloride threshold concentration for corrosion initiation in synthetic pore solutions, *Cem. Concr. Res.* 26 (1996) 545–550.
- [15] P. Ghods, O.B. Isgor, G. McRae, T. Miller, The effect of concrete pore solution composition on the quality of passive oxide films on black steel reinforcement, *Cem. Concr. Compos.* 31 (2009) 2–11.
- [16] H.E.H. Bird, B.R. Pearson, P.A. Brook, The breakdown of passive films on iron, *Corros. Sci.* 28 (1988) 81–86.
- [17] O.A. Kayyali, M.N. Haque, The Cl^-/OH^- ratio in chloride-contaminated concrete - a most important criterion, *Mag. Concr. Res.* 47 (1995) 235–242.
- [18] G.K. Glass, N.R. Buenfeld, The presentation of the chloride threshold level for corrosion of steel in concrete, *Corros. Sci.* 39 (1997) 1001–1013.
- [19] G.K. Glass, B. Reddy, N.R. Buenfeld, The participation of bound chloride in passive film breakdown on steel in concrete, *Corros. Sci.* 42 (2000) 2013–2021.
- [20] U.M. Angst, B. Elsener, C.K. Larsen, Ø. Vennesland, Chloride induced reinforcement corrosion: electrochemical monitoring of initiation stage and chloride threshold values, *Corros. Sci.* 53 (2011) 1451–1464.
- [21] G.K. Glass, N.R. Buenfeld, The inhibitive effects of electrochemical treatment applied to steel in concrete, *Corros. Sci.* 42 (2000) 923–927.
- [22] J.A. González, E. Otero, S. Feliu, W. López, Initial steps of corrosion in the steel/Ca(OH)₂ + Cl⁻ system: the role of heterogeneities on the steel surface and oxygen supply, *Cem. Concr. Res.* 23 (1993) 33–40.
- [23] J.S.J. van Deventer, J.L. Provis, P. Duxson, D.G. Brice, Chemical research and climate change as drivers in the commercial adoption of alkali activated materials, *Waste Biomass Valoriz.* 1 (2010) 145–155.
- [24] J.L. Provis, J.S.J. van Deventer (Eds.), *Alkali Activated Materials - State of the Art Report of RILEM TC 224-AAM*, Springer/RILEM, Dordrecht, 2014.
- [25] J.L. Provis, Geopolymers and other alkali activated materials: why, how, and what? *Mater. Struct.* 47 (2013) 11–25.
- [26] J.L. Provis, S.A. Bernal, Geopolymers and related alkali-activated materials, *Annu. Rev. Mater. Res.* 44 (2014) 299–327.
- [27] A. Vollpracht, B. Lothenbach, R. Snellings, J. Haufe, The pore solution of blended cements: a review, *Mater. Struct.* 49 (2016) 3341–3367.
- [28] R.R. Lloyd, J.L. Provis, J.S.J. van Deventer, Pore solution composition and alkali diffusion in inorganic polymer cement, *Cem. Concr. Res.* 40 (2010) 1386–1392.
- [29] P. Duxson, G.C. Lukey, F. Separovic, J.S.J. van Deventer, Effect of alkali cations on aluminum incorporation in geopolymeric gels, *Ind. Eng. Chem. Res.* 44 (2005) 832–839.
- [30] J.M. Miranda, A. Fernández-Jiménez, J.A. González, A. Palomo, Corrosion resistance in activated fly ash mortars, *Cem. Concr. Res.* 35 (2005) 1210–1217.
- [31] D.M. Bastidas, A. Fernández-Jiménez, A. Palomo, J.A. González, A study on the passive state stability of steel embedded in activated fly ash mortars, *Corros. Sci.* 50 (2008) 1058–1065.
- [32] M. Criado, D.M. Bastidas, S. Fajardo, A. Fernández-Jiménez, J.M. Bastidas, Corrosion behaviour of a new low-nickel stainless steel embedded in activated fly ash mortars, *Cem. Concr. Compos.* 33 (2011) 644–652.
- [33] C. Monticelli, M.E. Natali, A. Balbo, C. Chiavari, F. Zanotto, S. Manzi, M.C. Bignozzi, Corrosion behavior of steel in alkali-activated fly ash mortars in the light of their microstructural, mechanical and chemical characterization, *Cem. Concr. Res.* 80 (2016) 60–68.
- [34] M. Babae, A. Castel, Chloride-induced corrosion of reinforcement in low-calcium fly ash-based geopolymer concrete, *Cem. Concr. Res.* 88 (2016) 96–107.
- [35] R.J. Myers, S.A. Bernal, J.L. Provis, A thermodynamic model for C-(N)-A-S-H gel: CNASH.ss. Derivation and validation, *Cem. Concr. Res.* 66 (2014) 27–47.
- [36] C. Andrade, C. Alonso, Corrosion rate monitoring in the laboratory and on-site, *Constr. Build. Mater.* 10 (1996) 315–328.
- [37] D.D. MacDonald, B. Roberts, The cyclic voltammetry of carbon steel in concentrated sodium hydroxide solution, *Electrochim. Acta* 23 (1978) 781–786.
- [38] B. Kabanov, R. Burstein, A. Frumkin, Kinetics of electrode processes on the iron electrode, *Discuss. Faraday Soc.* 1 (1947) 259–269.
- [39] M. Jayalakshmi, V.S. Muralidharan, Passivation and hydrogen evolution studies on iron in alkali solutions, *Corros. Rev.* 12 (1994) 305–320.
- [40] R.S. Schrebler Guzman, J.R. Vilche, A.J. Arvia, The voltammetric detection of intermediate electrochemical processes related to iron in alkaline aqueous solutions, *J. Appl. Electrochem.* 11 (1981) 551–561.
- [41] R.S. Schrebler Guzman, J.R. Vilche, A.J. Arvia, The potentiodynamic behaviour of iron in alkaline solutions, *Electrochim. Acta* 24 (1979) 395–403.
- [42] D.M. Drazic, C.S. Hao, Anodic processes on an iron electrode in neutral electrolytes, *Doc. Chem. Yugosl.* 47 (1982) 649–659.
- [43] J.O. Bockris, S.U.M. Khan, *Surface Electrochemistry: A Molecular Level Approach*, Springer Science & Business Media, 2013.
- [44] H. Neugebauer, G. Nauer, N. Brinda-Konopik, G. Gidaly, The in situ determination of oxidation products on iron electrodes in alkaline electrolytes using multiple internal reflection Fourier transform infrared spectroscopy, *J. Electroanal. Chem. Interfacial Electrochem.* 122 (1981) 381–385.
- [45] E. Volpi, A. Olietti, M. Stefanoni, S.P. Trasatti, Electrochemical characterization of mild steel in alkaline solutions simulating concrete environment, *J. Electroanal. Chem.* 736 (2015) 38–46.
- [46] L. Freire, X.R. Nóvoa, M.F. Montemor, M.J. Carmezim, Study of passive films formed on mild steel in alkaline media by the application of anodic potentials, *Mater. Chem. Phys.* 114 (2009) 962–972.
- [47] L.D. Burke, M.E.G. Lyons, The formation and stability of hydrous oxide films on iron under potential cycling conditions in aqueous solution at high pH, *J. Electroanal. Chem.* 198 (1986) 347–368.
- [48] W. Tschinkel, H. Neugebauer, A. Neckel, In situ FTIR spectroscopy of iron electrodes in alkaline solutions II. External reflection absorption spectroscopy, *J. Electrochem. Soc.* 137 (1990) 1475–1480.
- [49] D.D. Macdonald, D. Owen, The electrochemistry of iron in 1M lithium hydroxide solution at 22° and 200 °C, *J. Electrochem. Soc.* 120 (1973) 317–324.
- [50] D.A. Harrington, P. Van Den Driessche, Mechanism and equivalent circuits in electrochemical impedance spectroscopy, *Electrochim. Acta* 56 (2011) 8005–8013.
- [51] L.F. Lin, C.Y. Chao, D.D. Macdonald, A point defect model for anodic passive films II. Chemical breakdown and pit initiation, *J. Electrochem. Soc.* 128 (1981) 1194–1198.
- [52] M. Sánchez, J. Gregori, C. Alonso, J.J. García-Jareño, H. Takenouti, F. Vicente, Electrochemical impedance spectroscopy for studying passive layers on steel rebars immersed in alkaline solutions simulating concrete pores, *Electrochim. Acta* 52 (2007) 7634–7641.
- [53] J.R. MacDonald, *Impedance Spectroscopy: Emphasizing Solid Materials and Systems*, Wiley-Interscience, 1987.
- [54] P. Ghods, O.B. Isgor, G.A. McRae, G.P. Gu, Electrochemical investigation of chloride-induced depassivation of black steel rebar under simulated service conditions, *Corros. Sci.* 52 (2010) 1649–1659.
- [55] G.T. Burstein, P.C. Pistorius, S.P. Mattin, The nucleation and growth of corrosion pits on stainless-steel, *Corros. Sci.* 35 (1993) 57–62.
- [56] N.J.J. Laycock, R.C.C. Newman, Localised dissolution kinetics, salt films and pitting potentials, *Corros. Sci.* 39 (1997) 1771–1790.
- [57] U. Angst, B. Elsener, C.K. Larsen, Ø. Vennesland, Chloride induced reinforcement corrosion: rate limiting step of early pitting corrosion, *Electrochim. Acta* 56 (2011) 5877–5889.
- [58] M. Moreno, W. Morris, M.G. Alvarez, G.S. Duffó, Corrosion of reinforcing steel in simulated concrete pore solutions, *Corros. Sci.* 46 (2004) 2681–2699.
- [59] U. Angst, A. Rönquist, B. Elsener, C.K. Larsen, Ø. Vennesland, Probabilistic considerations on the effect of specimen size on the critical chloride content in

- reinforced concrete, *Corros. Sci.* 53 (2011) 177–187.
- [60] S.M. Abd El Haleem, S. Abd El Wanees, E.E. Abd El Aal, A. Diab, Environmental factors affecting the corrosion behavior of reinforcing steel. IV. Variation in the pitting corrosion current in relation to the concentration of the aggressive and the inhibitive anions, *Corros. Sci.* 52 (2010) 1675–1683.
- [61] F. Zhang, J. Pan, C. Lin, Localized corrosion behaviour of reinforcement steel in simulated concrete pore solution, *Corros. Sci.* 51 (2009) 2130–2138.
- [62] A. Poursaei, C.M. Hansson, Reinforcing steel passivation in mortar and pore solution, *Cem. Concr. Res.* 37 (2007) 1127–1133.
- [63] J. Williamson, O.B. Isgor, The effect of simulated concrete pore solution composition and chlorides on the electronic properties of passive films on carbon steel rebar, *Corros. Sci.* 106 (2016) 82–95.
- [64] D.A. Hausmann, Steel corrosion in concrete: how does it occur? *Mater. Prot.* 6 (1967) 19–23.